Check for updates

Climate impacts on global agriculture emerge earlier in new generation of climate and crop models

Jonas Jägermeyr [1,2,3 ✉], Christoph Müller [3], Alex C. Ruane [1], Joshua Elliott[4], Juraj Balkovic[5,6], Oscar Castillo[7], Babacar Faye[8], Ian Foster [9], Christian Folberth [5], James A. Franke[4,10], Kathrin Fuchs[11], Jose R. Guarin [1,2], Jens Heinke[3], Gerrit Hoogenboom [7,12], Toshichika Iizumi [13], Atul K. Jain [14], David Kelly[9], Nikolay Khabarov [5], Stefan Lange [3], Tzu-Shun Lin [14], Wenfeng Liu[15], Oleksandr Mialyk [16], Sara Minoli[3], Elisabeth J. Moyer [4,10], Masashi Okada[17], Meridel Phillips[1,2], Cheryl Porter [7], Sam S. Rabin[11,18], Clemens Scheer[11], Julia M. Schneider [19], Joep F. Schyns [16], Rastislav Skalsky [5,20], Andrew Smerald [11], Tommaso Stella [21], Haynes Stephens [4,10], Heidi Webber [21], Florian Zabel [19] and Cynthia Rosenzweig [1]

Potential climate-related impacts on future crop yield are a major societal concern. Previous projections of the Agricultural Model Intercomparison and Improvement Project's Global Gridded Crop Model Intercomparison based on the Coupled Model Intercomparison Project Phase 5 identified substantial climate impacts on all major crops, but associated uncertainties were substantial. Here we report new twenty-first-century projections using ensembles of latest-generation crop and climate models. Results suggest markedly more pessimistic yield responses for maize, soybean and rice compared to the original ensemble. Mean end-of-century maize productivity is shifted from +5% to −6% (SSP126) and from +1% to −24% (SSP585)—explained by warmer climate projections and improved crop model sensitivities. In contrast, wheat shows stronger gains (+9% shifted to +18%, SSP585), linked to higher CO_2 concentrations and expanded high-latitude gains. The 'emergence' of climate impacts consistently occurs earlier in the new projections—before 2040 for several main producing regions. While future yield estimates remain uncertain, these results suggest that major breadbasket regions will face distinct anthropogenic climatic risks sooner than previously anticipated.

C limate change already affects agricultural productivity worldwide via many mechanisms, driven largely by warmer mean and extreme temperatures, altered precipitation regimes and drought patterns, and elevated atmospheric CO_2 concentrations ($[CO_2]$)[1]. Uncertainties arising from greenhouse gas emission scenarios, climate model projections and the understanding and representation of complex impact processes render estimates of future crop yield highly uncertain[2]. A way towards improving yield projections is the development of benchmarked multi-model ensemble simulations driven by harmonized simulation protocols[3]. Facilitated by the Agricultural Model Intercomparison and Improvement Project

(AgMIP)[4] and the Inter-Sectoral Impact Model Intercomparison Project (ISIMIP)[5], here we present a new systematic assessment of agricultural yield projections, based on a protocol similar to the one used by the Coupled Model Intercomparison Project (CMIP) for climate models[6].

In 2014, AgMIP's Global Gridded Crop Model Intercomparison (GGCMI) provided the first set of harmonized crop model projections based on CMIP5 (GGCMI–CMIP5; hereafter 'GC5'), which identified substantial climate impacts on all major crops, but also demonstrated that crop models might indeed introduce larger uncertainty than climate models[7]. CMIP6 now provides new

[1]NASA Goddard Institute for Space Studies, New York, NY, USA. [2]Columbia University, Center for Climate Systems Research, New York, NY, USA. [3]Potsdam Institute for Climate Impacts Research (PIK), Member of the Leibniz Association, Potsdam, Germany. [4]Center for Robust Decision-making on Climate and Energy Policy (RDCEP), University of Chicago, Chicago, IL, USA. [5]International Institute for Applied Systems Analysis, Laxenburg, Austria. [6]Faculty of Natural Sciences, Comenius University in Bratislava, Bratislava, Slovak Republic. [7]Agricultural & Biological Engineering Department, University of Florida, Gainesville, FL, USA. [8]Institut de recherche pour le développement (IRD) ESPACE-DEV, Montpellier, France. [9]Department of Computer Science, University of Chicago, Chicago, IL, USA. [10]Department of the Geophysical Sciences, University of Chicago, Chicago, IL, USA. [11]Institute of Meteorology and Climate Research, Atmospheric Environmental Research, Karlsruhe Institute of Technology, Garmisch-Partenkirchen, Germany. [12]Institute for Sustainable Food Systems, University of Florida, Gainesville, FL, USA. [13]Institute for Agro-Environmental Sciences, National Agriculture and Food Research Organization, Tsukuba, Japan. [14]Department of Atmospheric Sciences, University of Illinois, Urbana, IL, USA. [15]Center for Agricultural Water Research in China, College of Water Resources and Civil Engineering, China Agricultural University, Beijing, China. [16]Multidisciplinary Water Management group, University of Twente, Enschede, Netherlands. [17]Center for Climate Change Adaptation, National Institute for Environmental Studies, Tsukuba, Japan. [18]Department of Environmental Sciences, Rutgers University, New Brunswick, NJ, USA. [19]Ludwig-Maximilians-Universität München (LMU), Munich, Germany. [20]Soil Science and Conservation Research Institute, National Agricultural and Food Centre, Bratislava, Slovak Republic. [21]Leibniz Centre for Agricultural Landscape Research (ZALF), Müncheberg, Germany. ✉e-mail: jonas.jaegermeyr@columbia.edu
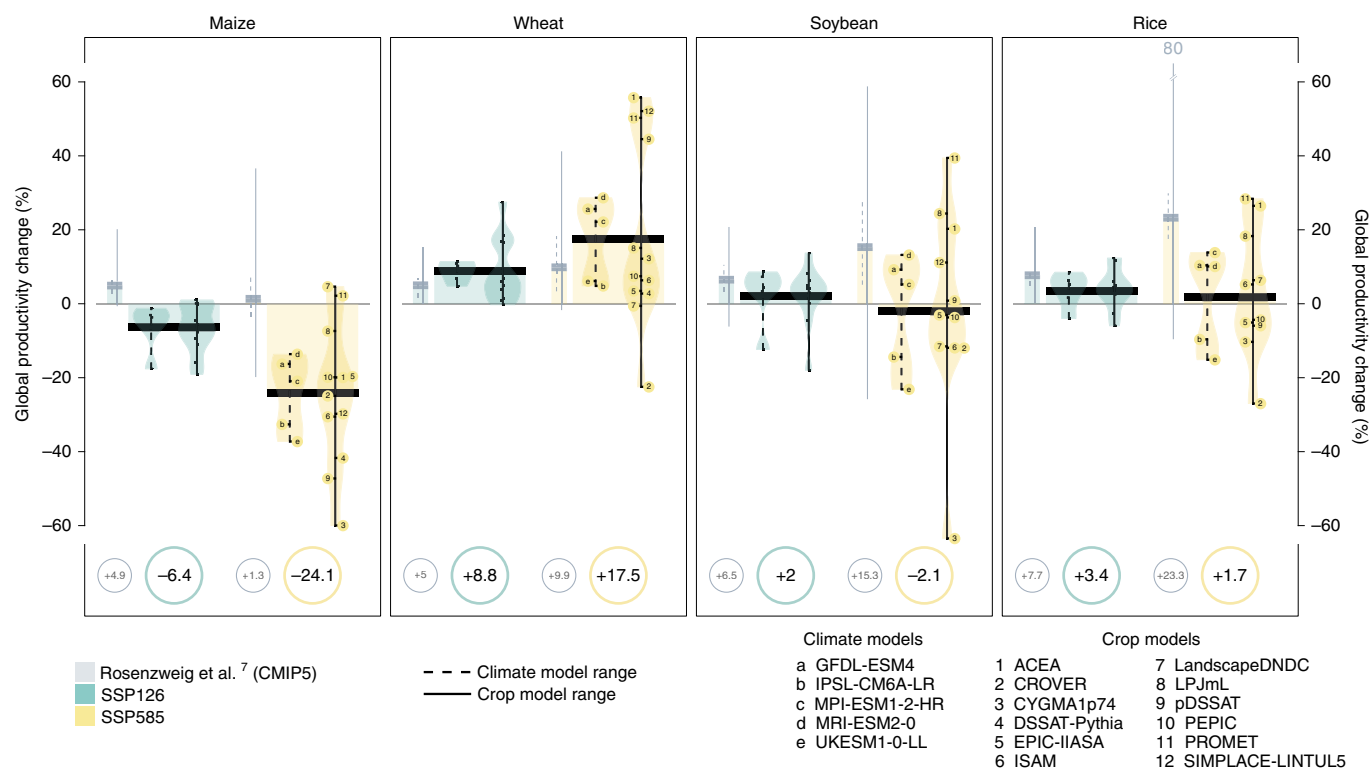
Fig. 1 | Ensemble end-of-century crop productivity response. Global productivity changes (2069–2099 compared to 1983–2013) for SSP126 and SSP585 are shown as the mean across climate and crop models for the four major crops (highlighted by numbers in circles underneath each plot). Whiskers indicate the range of individual climate model realizations (dashed line, as the mean across crop models), and the range across crop models (solid line, as the mean across climate models). Individual model results are indicated by the bullets along the whisker lines (for SSP585 only); violin shades additionally highlight the model distribution. For context, grey bars and whiskers reference previous GGCMI simulations based on CMIP5 (GC5; Rosenzweig et al.[7]) in the same way, without specifying individual models. Data are shown for the default [CO_2]. Not all crop models simulate all crops, see Supplementary Table 3 for details.

reference climate projections[8,9], and improved bias-adjustment and downscaling methods[10] benefit the impact modelling community. With improved and further harmonized inputs and cropping system configurations, and an advanced ensemble of state-of-the-art process-based crop models, GGCMI is able to provide a new standard in global crop yield projections for the twenty-first century for several major crops using CMIP6 climate scenarios (GGCMI–CMIP6; hereafter 'GC6').

Climate change impacts are usually quantified in terms of differences over time, but especially in view of adaptation measures, it is the amplitude of the change compared to the local background variability and uncertainty of the recent past that is often relevant[11]. Time of climate impact emergence (TCIE)—the point in time by which the yield levels of exceptional years (negative or positive) have become the new norm—is a critical measure for risk assessment. Time of emergence[12] metrics have been applied to climate variables including temperature[13], precipitation[14] and others[15,16] and demonstrate that major food-producing regions are increasingly facing changing climate profiles in the near term. Here we introduce the TCIE concept with respect to future agricultural risks.

Recent literature has focused on capturing the temperature sensitivity of crops in isolation[17–19]. To quantify climate change impacts more comprehensively, additional factors including precipitation changes, temperature–moisture feedbacks and [CO_2] need to be considered. The projections presented here dynamically respond to these climate drivers and shed new light on the effects of elevated [CO_2], which are among the largest sources of uncertainty in long-term crop yield estimates[20–22].

As the first update since GC5 in 2014[7], the aims of this initial GC6 study are: (1) to provide latest-generation ensemble projections for the productivity of major crops for the twenty-first century, (2) to assess climate change impacts on crop yields from a risk perspective, employing the TCIE concept, (3) to improve understanding of regional patterns of change and (4) to explore drivers of uncertainty related to climate models, crop models and responses to [CO_2].

Global production response of major crops

The simulation protocol is based on two representative concentration pathways (RCPs), RCP2.6 and RCP8.5 (hereafter 'SSP126' and 'SSP585'; adaptation measures associated with the shared socioeconomic pathways are not considered)[9], chosen to sample the range of available scenarios and to make the results comparable with GC5. Twelve GGCMs each simulated five GCM forcings, resulting in about 240 climate–crop model realizations per crop (GGCMs × GCMs × RCPs × CO_2 settings). The climate projections from the five GCMs (Supplementary Table 1), bias-adjusted and downscaled, are selected by ISIMIP based on benchmark performance, equilibrium climate sensitivity and output availability (Methods). All simulations are carried out globally on a 0.5° grid, covering the time period 1850–2100 and we evaluate results based on transient atmospheric [CO_2] (that is, 'default [CO_2]'). This study is based on temporally constant management assumptions, focusing on the isolated climate change effect on current crop production systems.

The ensemble response across the new generation of climate and crop models to the SSP126 and SSP585 forcing is markedly more pronounced than in GC5 (ref.[7]) (Fig. 1). Wheat results are more optimistic, while maize, soybean and rice results are decisively more pessimistic. For maize, the most important global crop in terms of total production and food security in many regions, the mean end-of-century (2069–2099) global productivity response is ~10%
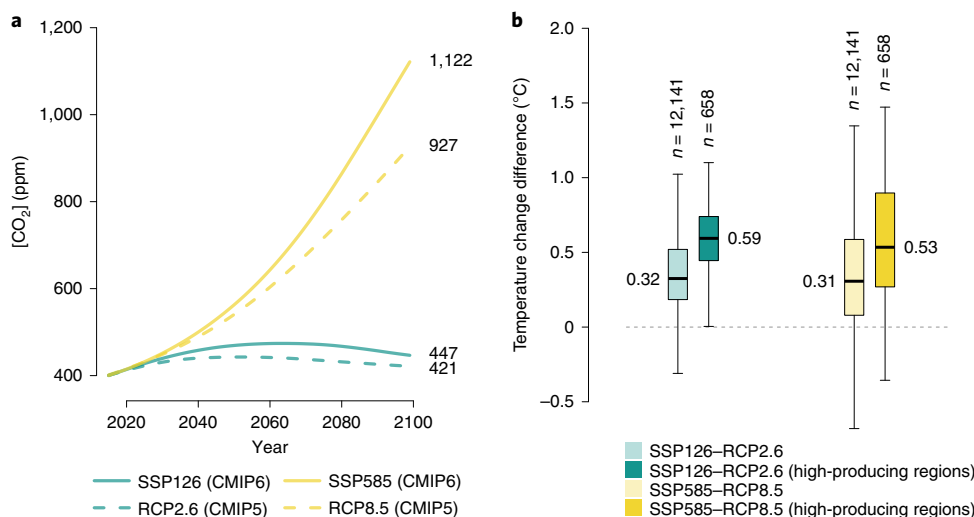
Fig. 2 | Comparison of [CO₂] and temperature changes between CMIP5 and CMIP6. a, [CO₂] pathways for RCP2.6 and RCP8.5 in CMIP5 compared to SSP126 and SSP585 in CMIP6. **b**, Box-and-whisker plots showing the difference of the average maize growing season temperature changes (2069–2099 versus 1983–2013) between the CMIP6 and CMIP5 ensembles. Each ensemble is represented by the mean of five GCMs (Supplementary Tables 1 and 2) in each grid cell. CMIP6 and CMIP5 differences are separated for SSP126 (green) and SSP585 (yellow) for all maize-producing grid cells (lighter shade) and for the highest-producing grid cells that together account for 50% of global production (darker shade).

(SSP126) and ~20% (SSP585) lower than in GC5. This shifts the SSP585 estimate from +1% (interquartile range (IQR) of crop–climate model combinations: −10% to +8%) to −24% (IQR: −38% to −7%) and for SSP126 from +5 to −6%.

For wheat, the second largest global crop in terms of production, the SSP585 ensemble estimate is shifted upwards from +10% (IQR: −1% to +15%) to +18% (IQR: −2% to +39%), and under SSP126 from +5% to +9%. The SSP585 ensemble estimates for soybean are revised downward from +15% (IQR: −8% to +36%) to −2% (IQR: −21% to +17%) and for rice from +23% (IQR: +1% to +33%) to +2% (IQR: −15% to +12%). Overall, the new climate and crop model combinations narrow the range of crop yield projections for soybean and rice, but disagreement among crop models remains substantial and is largely indecisive about the sign of change at the global level (t test: $P > 0.5$ for both crops). The maize and wheat responses are robust and became more distinct since GC5. While the range of crop projections somewhat increased, 85% of model combinations indicate negative maize changes and 73% project positive wheat changes under SSP585. Both responses are now statistically significant ($P < 10^{-5}$); the maize response in GC5 was not ($P > 0.6$). There is larger agreement on positive change for wheat under SSP126 (89%) than under SSP585, indicating peak-and-decline trajectories for parts of the ensemble under high-emissions scenarios (Supplementary Fig. 1).

As a C₄ crop, maize has a smaller capacity to benefit from elevated [CO₂] (ref. [23]), and is also grown across a wider range of low latitudes that are projected to experience the largest adverse impacts due in large part to current proximity to crop-limiting temperature thresholds[24]. As a C₃ crop, the positive wheat response is explained by its relatively stronger CO₂ response and the fact that global warming leads to wheat yield increases in high-latitude regions that are currently temperature-limited[19].

Three factors explain the more pronounced crop yield response in GC6. First, CMIP6 has markedly higher [CO₂] than CMIP5 (Fig. 2), with year 2099 concentrations increased from 927 ppm (RCP8.5) to 1,122 ppm (SSP585)[9]. Second, CMIP6 has higher average end-of-century warming levels than CMIP5, adequately represented in the five GCMs sampled here (Supplementary Tables 1 and 2). While both RCP2.6 and RCP8.5 are on average ~0.3 °C warmer in CMIP6 than in CMIP5 over land and oceans, the

difference is even more pronounced (>0.5 °C) across the main maize-producing regions (Fig. 2). Third, the new crop model ensemble features advanced versions of previous models, several new members and improved input data, which resulted in more realistic sensitivities to climate and [CO₂] changes (see details below).

Emergence of the climate change signal in agriculture

The TCIE describes the point in time when average climate change impacts are projected to occur outside the envelope of historical variability and uncertainty ('noise'). We define TCIE as the year in which the multi-model 25 yr moving-average crop production change ('signal') emerges from the noise (that is, the standard deviation of simulated variability across all GCM×GGCM combinations in 1983–2013).

Maize consistently shows emerging negative productivity changes ('negative TCIE') among major producer regions. The ensemble median signal emerges from the noise at the global level in the year 2032 under SSP585 and in the year 2051 under SSP126 (Fig. 3). Of all individual GCM×GGCM realizations, 84% show a negative TCIE by 2099 under SSP585 (52% under SSP126) and the IQR spans from 2014 to 2056, indicating sizeable agreement among models. This is a substantial shift away from the GC5 simulations in which the ensemble median shows no emergence by 2099 under any emission pathway, only seen in 46% of individual GCM×GGCM combinations under RCP8.5 (IQR: 2044–2080). Overall, the TCIE signal at the global level is shifted earlier and is more pronounced in the new generation of climate and crop model projections (Fig. 4).

By the end of the century, 10% (SSP126) to 74% (SSP585) of current global maize cultivation areas are projected to undergo negative TCIE (Fig. 5). Under SSP585 this trajectory is markedly earlier, with higher late-century fractions of cropland area affected compared to the respective 47% in GC5 (RCP8.5). Crop models indicate early negative maize TCIE before 2040 even under SSP126 in Central Asia, the Middle East, southern Europe, the western United States and tropical South America. Projections referencing the 1983–2013 period suggest that the mean yield signal is already starting to emerge in some of these regions (Figs. 3e and 5), patterns largely in line with recent observations[14,25,26].

The standard deviation of grid-level TCIE estimates under SSP585 ranges between 25 and 35 yr across most breadbasket
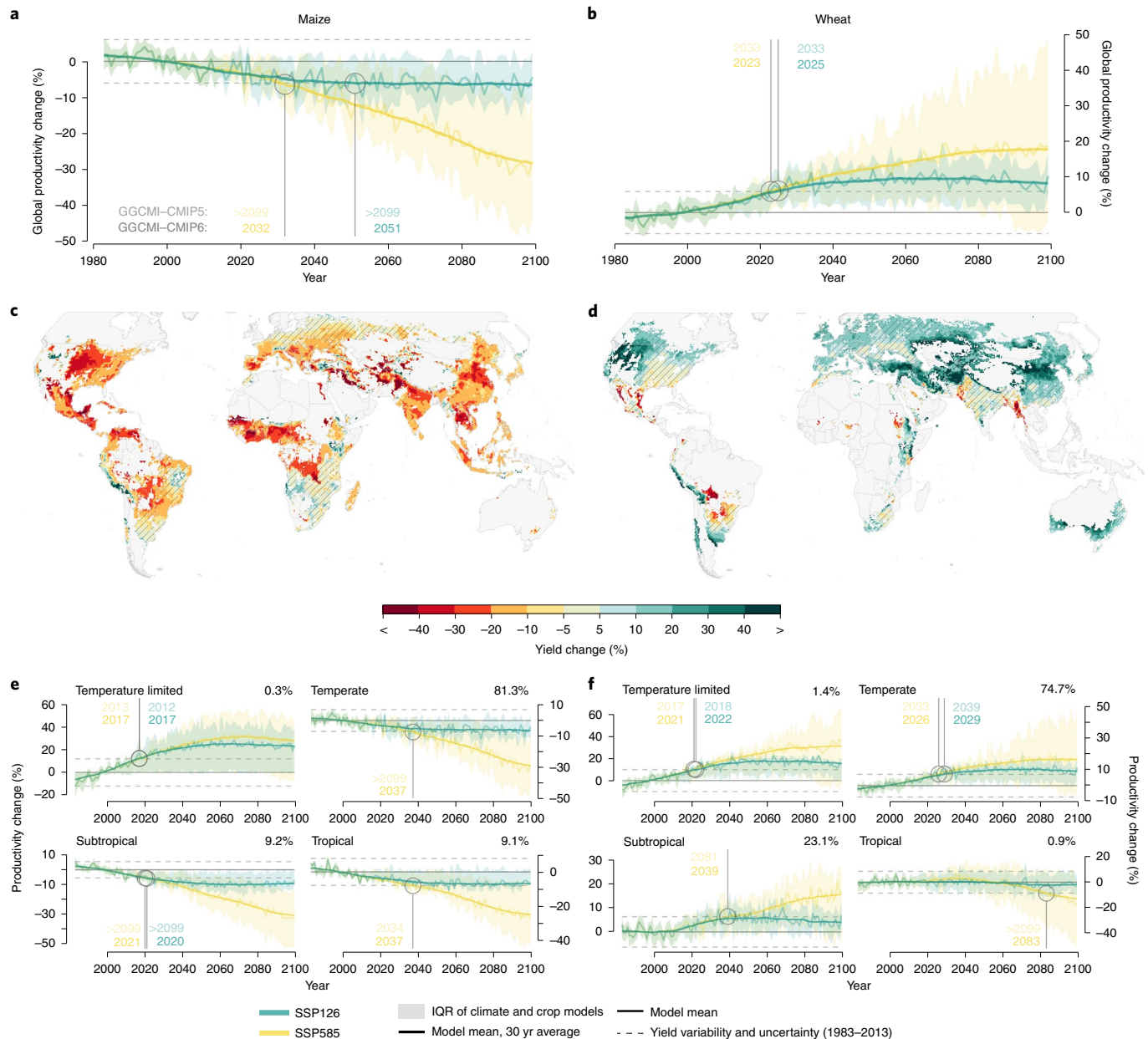
Fig. 3 | Projections of global crop productivity for the twenty-first century. a,b, Productivity time series for maize (**a**) and wheat (**b**) shown as relative changes to the 1983–2013 reference period under SSP126 (green) and SSP585 (yellow). Shaded ranges illustrate the IQR of all climate–crop model combinations (5 GCMs × 12 GGCMs). The solid line shows the median response (and a 25 yr moving average). Horizontal dashed lines mark the standard deviation of historical yield variability and model uncertainty (that is, 'noise' from individual climate–crop model combinations) and open circles highlight the TCIE, the year in which the smoothed climate change response emerges from the noise. For context, the TCIE calculated from GC5 (ref. [7]) simulations is indicated in lighter shades above the TCIE based on GC6 (>2099 if no TCIE occurs by 2099). **c,d**, Maps showing median yield changes (2069–2099) for maize (**c**) and wheat (**d**) under SSP585 across climate and crop models for current growing regions (>10 ha). Hatching indicates areas where <70% of the climate–crop model combinations agree on the sign of impact. **e,f**, Regional productivity time series for maize (**e**) and wheat (**f**) similar to **a**, but stratified for the four major Koeppen–Geiger climate zones (temperature limited, temperate/humid, subtropical and tropical). The percentage of the total global production contributed by each zone is indicated in the top right corner of the insets. All data are shown for the default [CO$_2$] (see Supplementary Fig. 3 for all four crops).

regions, with slightly higher values under SSP126 (Supplementary Fig. 2). Such uncertainty ranges are in line with time of emergence estimates for climatological variables, yet somewhat higher due to the additional layer of crop model uncertainties[12,13]. Clearest emergence signals, that is, largest signal-to-noise ratios with values <−2, are found among lower latitudes in the tropics but also in Central Asia, the Middle East and the western United States (Supplementary

Fig. 2e). As internal variability—and thus total noise—decreases with averaging, earlier TCIE is generally found for larger spatial scales.

For wheat, ensemble projections indicate TCIE of positive productivity changes ('positive TCIE') at the global level (Fig. 3b) and across large parts of currently cultivated areas (Fig. 5). While also found in GC5 simulations, TCIE is shifted ~10 yr earlier in GC6,
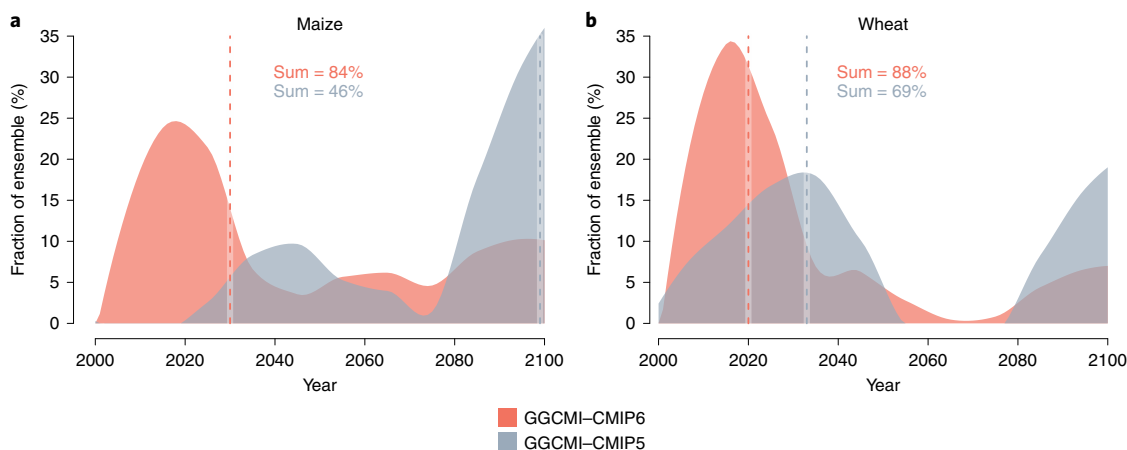
Fig. 4 | Shift towards earlier and more pronounced climate impact emergence. a,b, Density plots of individual TCIE estimates across the GCM × GGCM ensemble under SSP585 are shown for global maize productivity (**a**; negative TCIE) and global wheat productivity (**b**; positive TCIE). Histogram counts are smoothed with a locally weighted fit (LOESS; span, 0.5) and shown as the fraction of the respective ensemble size. The GGCMI–CMIP6 ensemble includes 12 crop models, GGCMI–CMIP5 includes seven crop models; both comprise five GCMs. The total ensemble fraction that shows TCIE by 2099 is indicated by 'Sum'. The ensemble median TCIE is highlighted with vertical dashed lines. See Supplementary Fig. 4 for soybean and rice.
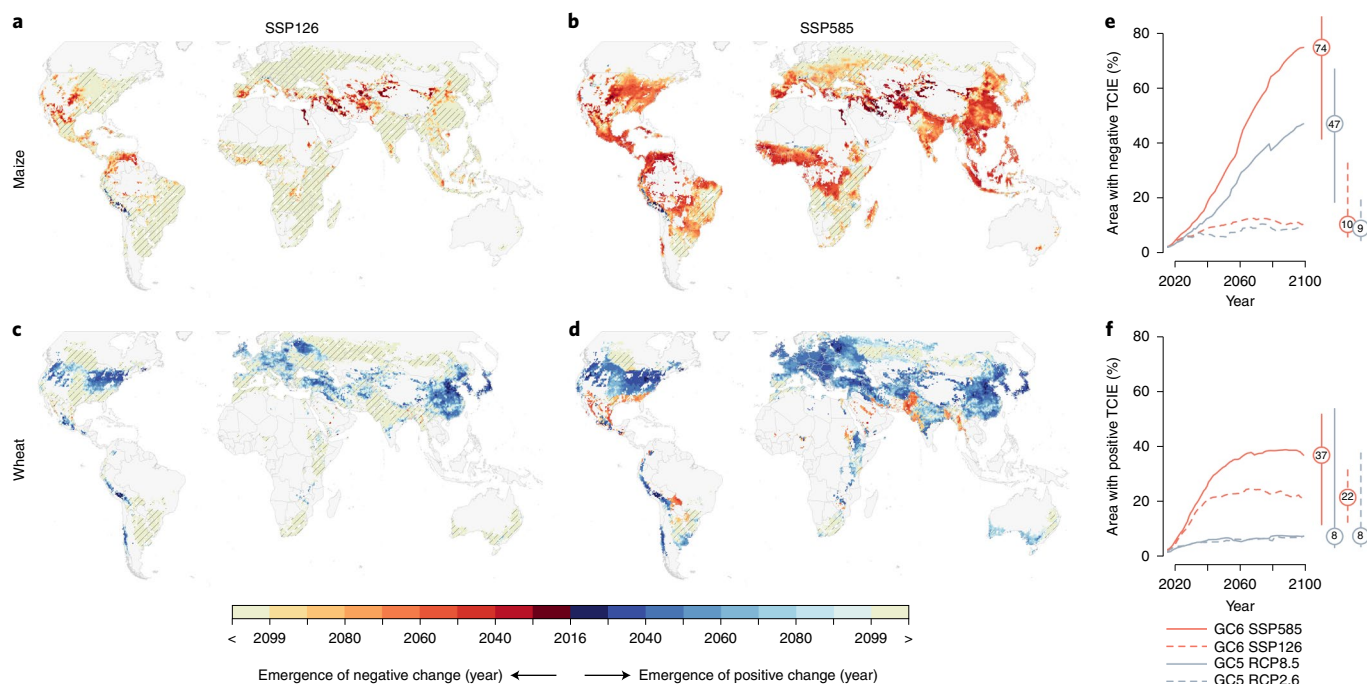

Fig. 5 | Geographic patterns in TCIE. a–d, Maps showing TCIE estimates for maize (**a,b**) and wheat (**c,d**) under SSP126 (**a,c**) and SSP585 (**b,d**)—calculated as the median of individual TCIE estimates from each climate–crop model combination. Hatching indicates areas in which <70% of the crop models agree on the emergence signal by 2099. See Supplementary Fig. 2 for the associated standard deviation of TCIE estimates and the signal-to-noise ratio. **e,f,** Illustration of the annual percentage of the respective global cropland area affected by negative TCIE (**e**, maize) and positive TCIE (**f**, wheat) under SSP126 and SSP585, separated for results from GC5 (ref. [7]) and GC6. Vertical bars indicate the IQR of all climate–crop model combinations, with the median value in the circle. The maps show the first TCIE occurrence, even if the signal is reversed by late century (for example, parts of India for wheat; compare with Supplementary Fig. 2); estimates of the affected areas in **e** and **f** account for signal changes.

suggesting that climate-related increases might occur globally within the next few years (year 2023 under SSP585, year 2025 under SSP126; IQR, 2014–2029 and 2015–2029) and across major bread-basket regions within the next two decades (Fig. 5). In some regions we already detect a TCIE signal today, which is in line with the range of time of emergence estimates for temperature and precipitation[13,14]. Such effects are difficult to distinguish from rapidly chang-

ing management practices in observational data, but climate change impacts have been documented, for example, in Central and South Asia, northern China and the United States[25,27]. The TCIE estimates for wheat show high consistencies across the model ensemble—76% (SSP126) and 88% (SSP585) of individual model combinations show positive TCIE by 2099. As for maize, the TCIE signal is shifted earlier and is more pronounced in GC6 than in GC5 (Fig. 4).

The share of wheat cultivation areas projected to see positive TCIE increased substantially in GC6, from 8% (GC5, RCP8.5) to 37% (GC6, SSP585; Fig. 5f). This share levels off by midcentury, a result of peak-and-decline trajectories seen in some crop models (compare Fig. 5d and Supplementary Fig. 2f for regions that show TCIE early on but not by late century). Wheat also exhibits negative TCIE among important growing regions in South Asia, the southern United States, Mexico and parts of South America around midcentury. The uncertainty among grid-level TCIE estimates is generally higher for wheat than for maize and the extent of areas with very high signal-to-noise ratios (that is, >2) is smaller (Supplementary Fig. 2f).

Ensemble median soybean and rice productivity peak midcentury and decline towards the end of the century at the global level (Supplementary Fig. 3). The soybean response exhibits late-century negative TCIE (year 2096) under SSP585; rice, on the other hand, shows early positive TCIE (year 2030, SSP585) but late-century declines are not projected to reach the level of negative TCIE at the global level (38% of GCM×GGCM combinations under RCP8.5 indicate negative TCIE by 2099; Supplementary Fig. 4). Rice is the only crop in this study that indicates positive TCIE in the tropics, which drives early net global gains before productivity is simulated to decline again by about 2060 (Supplementary Fig. 3c). As for maize and wheat, the TCIE signal is shifted earlier and is more pronounced in GC6 than in GC5 (Supplementary Fig. 4).

Regional patterns of yield change

Projections of crop yield changes include regions of losses and gains for all crops (Fig. 3 and Supplementary Fig. 3). Global average responses can hide important regional changes, which are supported by strong crop model agreement. Maize projections show spatially homogeneous losses especially among main growing regions in North America, Mexico, West Africa, Central Asia and China, where crop model agreement is high (Fig. 3c). The high-latitude gains found in GC5 are not as prevalent in GC6 and are associated with high crop model uncertainty and low baseline yields. Wheat shows distinct geographic gradients with losses in spring wheat regions in Mexico, the southern United States, South America and South Asia, supported by good model agreement. Sizeable wheat gains are projected by many models for the North China Plains, Australia, Central Asia, the Middle East and for the winter-wheat-growing regions in the northern United States and Canada (Fig. 3d). Soybean shows the greatest losses in the main-producer regions—the United States, Brazil and Southeast Asia—paired with large gains across parts of China and generally higher latitudes (Supplementary Fig. 3). Major declines in rice yields are simulated in Central Asia, and gains in South Asia, northeastern China and South America. Both soybean and rice yield changes must be interpreted in view of the wide range in crop model ensemble results (Fig. 1 and Supplementary Fig. 3). A breakdown of yield responses for the top-ten producer countries per crop highlights a wide range of CO_2 effects embedded in the signal (Supplementary Figs. 5 and 6).

A latitudinal profile of yield changes under SSP585—simulated in all grid cells irrespective of the current cropland distribution—indicates that losses are most prevalent among low-latitude tropical regions with highest gains found at higher latitudes beyond 50° N and 30° S for all crops (Fig. 6). Maize exhibits widespread losses between 50° N and 30° S, while losses for the other crops are more concentrated in the tropics with a less distinct signal for soybean and rice. Major wheat breadbaskets are generally located at higher latitudes than maize, which further contributes to overall wheat gains when aggregated across currently cultivated areas. Although more than 90% of maize and wheat is currently produced in the temperate and subtropical climate zones, major yield losses will affect the livelihoods and food security of many smallholder farmers in the tropics. Overall, our results show that lower latitudes face

the largest losses for all crops, while higher latitudes see potential gains. These conclusions are in line with the IPCC AR5 (ref. [28]) and recent studies[7,29,30] and such uneven distribution of impacts may further increase regional disparities that are a 'reason for concern'[31] regarding climate change risks.

Drivers of more pronounced ensemble response

It is difficult to determine to what degree the differences in crop yield projections between GC6 and GC5 can be explained by the new atmospheric forcing, the new crop model ensemble or new input data. A subset of GC6 and GC5 crop models that participated in both ensembles (albeit in different versions) shows very similar responses compared with the respective full ensemble, suggesting that the crop model selection does not explain the differences (Fig. 7). Further, standardized comparisons of crop model responses to specific mean temperature increases over cropland areas ('warming sensitivity'; under constant [CO_2] conditions, but including changes in other climate variables) from 1 to 2 °C and from 2 to 3 °C, respectively, highlights that the isolated warming sensitivity in GC6 has substantially increased for maize (from 2–3% in GC5 to 8–9% in GC6) and decreased for wheat (from 7% to 3–6%; Fig. 7). With higher overall warming levels in CMIP6, net warming-related maize losses by 2069–2099 thus increased from 12% (4.6 °C maize cropland warming) to 30% (5 °C maize cropland warming) in GC6. Moreover, the CO_2 sensitivity at 500 and 700 ppm, but also net effects by the end of the century, have decreased for both maize and wheat. In summary, the more pessimistic maize response in GC6 can largely be attributed to a higher sensitivity to warming and a lower compensating effect due to CO_2 fertilization in the crop models, and to a smaller extent to the higher absolute warming levels in CMIP6. For wheat on the other hand, the more optimistic response in GC6 can be explained by lower losses per degree warming (with stronger temperature-related gains in high-latitude regions), overcompensating for a lower CO_2 fertilization effect than in GC5 (despite higher total [CO_2] levels). For soybean and rice, in contrast, the more pessimistic response in GC6 is largely attributed to higher warming levels in CMIP6 compounded by a higher crop model sensitivity to warming, with similar sensitivities to changes in [CO_2] (Supplementary Fig. 7).

Crop and climate model uncertainty

The range of crop model responses under SSP585 (mean across climate models) is substantially larger than the range introduced by the five climate models (mean across crop models; Fig. 1). However, for all crops and RCPs, the uncertainty associated with the five CMIP6 climate models has increased compared to the five climate models sampled in GC5. In turn, the fraction of total variance induced by the crop models is substantially reduced for all crops in GC6 (for maize from 97% to 69%; Fig. 8), which highlights that the crop response became more consistent, despite the fact that the number of crop models increased. Absolute variance induced by the climate models has increased for all crops (Fig. 8), which is explained by a wider distribution of climate sensitivities tracked by the five CMIP6 GCMs (Supplementary Tables 1 and 2), but also by higher [CO_2] assumed in CMIP6 (Fig. 2). In this sample, UKESM1 is the most pessimistic GCM for both RCPs and all crops, the global mean warming level by 2099 is ~2.6 °C higher than in GFDL-ESM4, and the transient climate response is 1.2 °C higher (see Supplementary Table 1 for more details)[6]. Generally, the least pessimistic crop impacts are found with MRI-ESM2 (Fig. 1).

Higher emission scenarios inflate the crop model uncertainty (SSP585), while the overall climate- and crop model-induced uncertainty range in GC6 is of comparable size under SSP126 (Fig. 1). Uncertainty in the CO_2 effect causes much of the crop model uncertainty for wheat, soybean and rice (Supplementary Fig. 8), yet the range of maize responses is not fundamentally reduced without
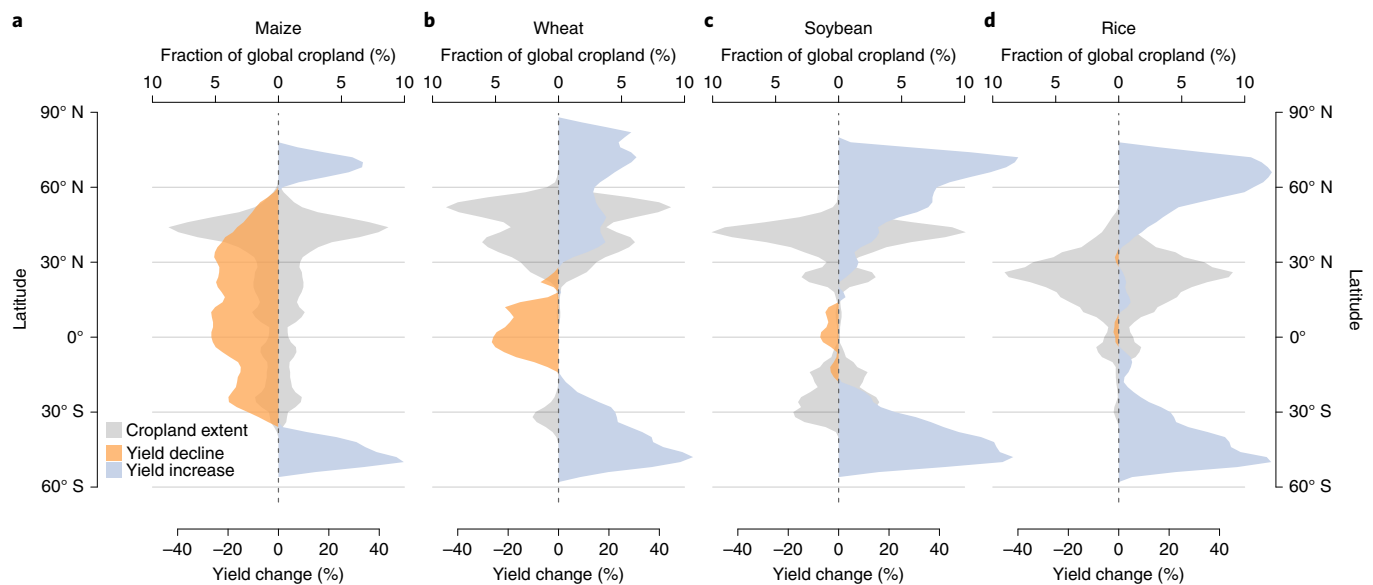
Fig. 6 | Latitudinal profile of crop yield changes. a–d, Yield changes (SSP585, 2069–2099) are shown as latitude averages for maize (**a**), wheat (**b**), soybean (**c**) and rice (**d**), based on crop simulations in all grid cells, unconstrained by current cropland extent (bottom *x* axis). For context, the current cropland extent is shown across latitude bands as fractions of the crop-specific global extent (top *x* axis; mirrored to allow overlaps with both positive and negative yield changes). Yield data are shown as the climate and crop model median (marginal areas with yield lower than the 20th percentile per crop are excluded).

the CO_2 effect. In line with physiological knowledge[23], crop models mostly show the smallest CO_2 effects for C_4 crops (maize) and much larger responses for C_3 crops (wheat, soybean, rice). However, the CO_2 effects differ widely across crop models; the ensemble median rainfed response is 19% for maize, 33% for wheat, 48% for soybean and 37% for rice by the year 2099 (Supplementary Fig. 8), which is generally in line with field experiments given that model simulations include nutrient limitations[20,23]. CYGMA and CROVER exhibit a strong peak-and-decline CO_2 response for some crops, resulting in negative CO_2 effects for maize in CYGMA after 2090 (Supplementary Fig. 8). This is driven by increased water use efficiencies under elevated [CO_2], eventually leading to adverse excess moisture effects in humid regions—a new feedback represented primarily in CYGMA and underexplored in previous studies[32].

In addition to the CO_2 effect, climate change affects simulations of crop growth and development in various ways. These include, for example, changed precipitation patterns, extreme heat and drought events, and importantly, accelerated maturity. Higher temperatures lead to faster phenological development and substantial reductions in the growing season length in all crop models, which in turn lead to complex processes affecting yield, including shorter grain-filling periods, smaller canopies and reductions in photosynthesis. This effect varies across models and additional work is needed to further narrow the range of crop model responses[33]. After all, the standard deviation of simulated yield variability matches observational data to a much higher degree in GC6 ($R = 79\%$) than in GC5 ($R = 44\%$), adding to more realistic yield responses (Supplementary Fig. 9).

Discussion
We introduce the concept of climate impact emergence to the field of agriculture impacts, highlighting that major shifts in global crop productivity due to climate change are projected to occur within the next 20 yr, several decades sooner than estimates based on previous model projections. The impact on crop productivity under SSP126 and SSP585 is largely similar for the coming decade, which leaves little room for climate mitigation efforts. In light of the much larger climate and crop model agreement for these short-term projections

than for the late century, the findings highlight challenges for food system adaptation faced with noticeably shorter lead times.

These CMIP6 multi-model crop yield projections suggest that climate change impacts on global agriculture will be more pronounced than in GC5, with substantially larger losses for maize, soybean and rice and additional gains for wheat. This is supported by a generally more consistent crop model ensemble. However, large uncertainties remain, particularly in TCIE estimates—the standard deviation for global maize TCIE is 24 yr (SSP585), which is similar to estimates of temperature emergence[12]. Yet the signal is robust: more than 80% of the GCM-GGCM combinations indicate TCIE for maize and wheat by late century across major breadbaskets (SSP585). TCIE estimates based on different metrics qualitatively agree (for example, multi-model ensemble mean TCIE for maize is found in the year 2032, the median of individual GCM×GGCM estimates in the year 2027, and the mean in the year 2036). Leaving one crop model out at a time introduces a TCIE standard deviation of only 1.5 yr for both maize and wheat (SSP585). That said, time of emergence estimates are sensitive to the underlying definitions (for example, noise, pre-industrial or recent climate, smoothing approach, threshold selection) and can push the emergence date earlier or later in time[12–14]. Absolute TCIE estimates are therefore more challenging to interpret than relative comparisons among regions, crops and especially the two ensemble projections GC5 and GC6.

Wheat yield increases are projected to level off by midcentury and part of the climate–crop model ensemble indicates net losses under SSP585 by 2099 (Fig. 1 and Supplementary Fig. 1). Maize yield, on the other hand, is projected to decline steadily, supported by higher model agreement than for wheat. These general response differences are also in line with previous findings[34]. The more pronounced response of the new projections can be explained primarily by higher equilibrium climate sensitivities, higher [CO_2] and different crop model sensitivities per degree warming and [CO_2] changes. With regard to CMIP6, higher and wider-ranging climate sensitivities are critically discussed and associated with differing parameterizations of cloud feedback and cloud–aerosol interactions[35–38]. While better simulations of cloud liquid water contents
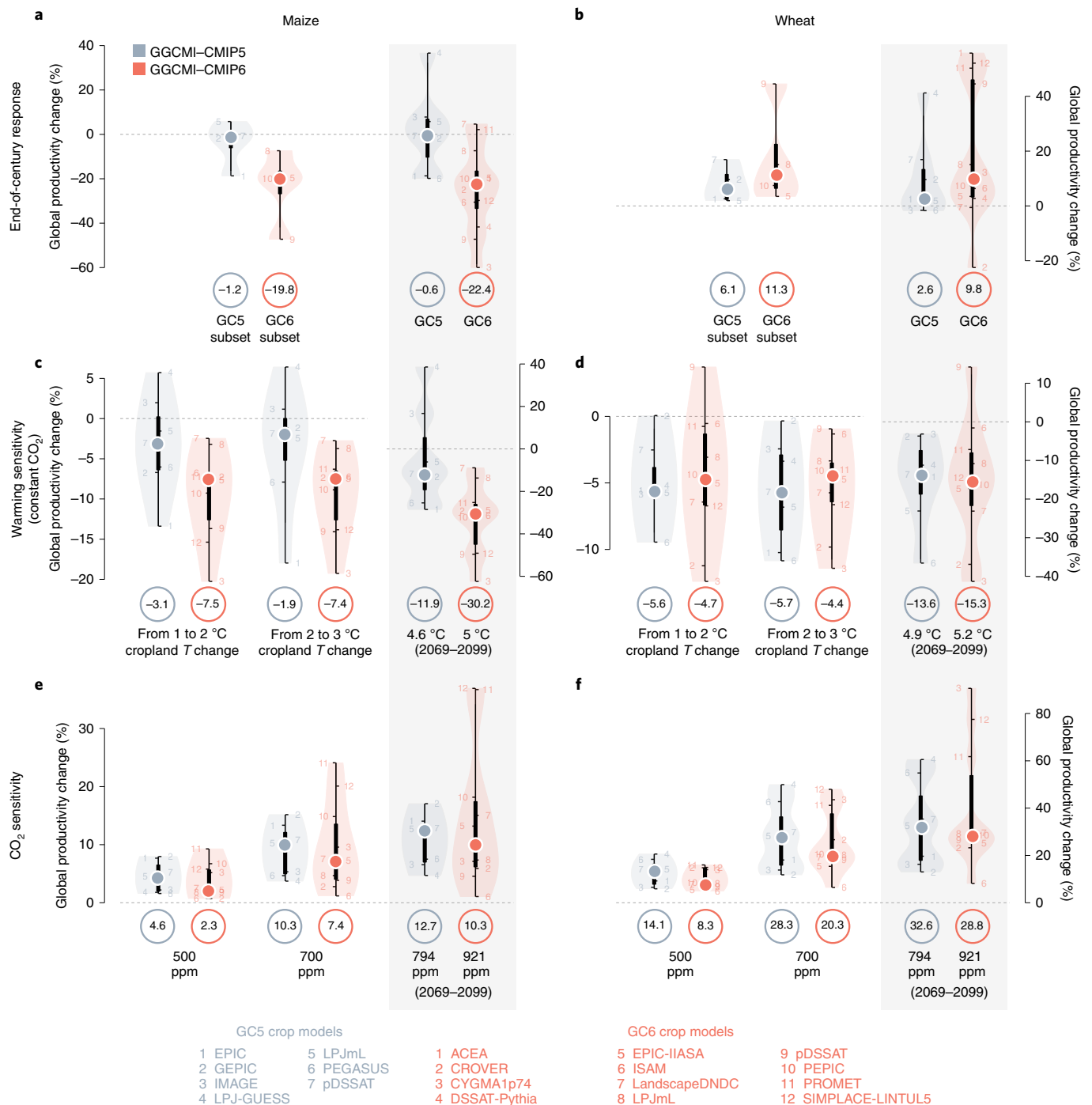
Fig. 7 | Driver attribution of crop model responses. a,b, Projected end-of-century global productivity changes for maize (**a**) and wheat (**b**) under RCP8.5 (climate model mean) are shown for all members of the crop model ensembles GGCMI–CMIP5 (GC5) and GGCMI–CMIP5 (GC6), and for a subset of crop models that participated in both rounds (note substantial differences between model versions). **c,d,** The sensitivity to global mean warming of the full ensembles is shown for temperature (*T*) changes over maize (**c**) and wheat (**d**) cropland areas from 1 to 2 °C, from 2 to 3 °C, and for the total change between 1983–2013 and 2069–2099. The warming sensitivity is based on [CO_2] held constant at the 2015 level but includes changes in other climate variables. **e,f,** The CO_2 sensitivity for maize (**e**) and wheat (**f**) in GC5 and GC6 is shown at specific [CO_2] and for the 2069–2099 mean concentrations. Warming and CO_2 sensitivities are calculated based on crop model responses over a 21 yr window centred on the year in which a certain temperature change or [CO_2] occurs in each climate model. Filled circles indicate the median crop model response, additionally highlighted by circled numbers underneath each plot. Black bars show the IQR and individual models are indicated by numbers. Note that both **c** and **d** include two different legends. See Supplementary Fig. 7 for soybean and rice results. ACEA and DSSAT-Pythia have not submitted simulations for the constant [CO_2] setting and are excluded from **c–f**.

and their radiative behaviour render the climate models more realistic, it is unclear whether these improvements translate into more accurate estimates of equilibrium climate sensitivity (ECS) and

overall warming levels. Additional improvements of the GCMs, and the bias-adjustment and downscaling methods used, result in better representations of extreme events and internal variability[10,39–41],
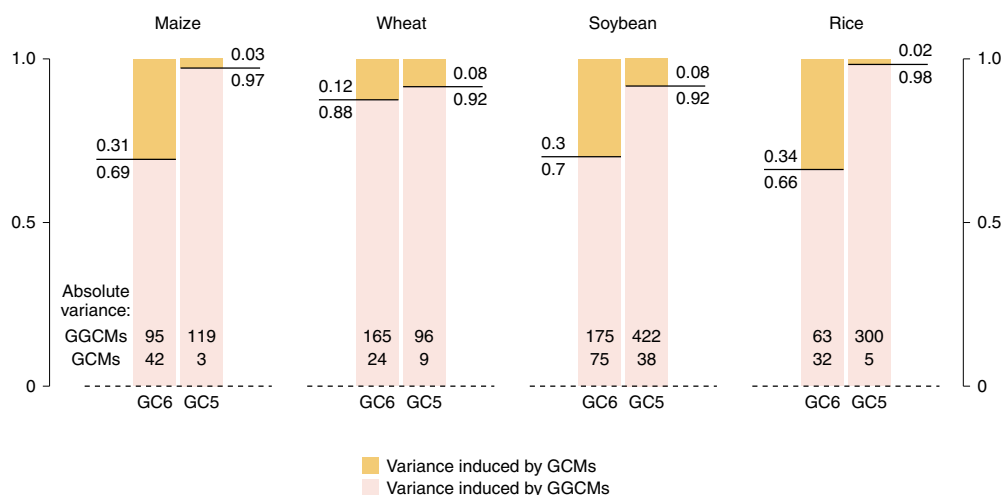
Fig. 8 | Variance decomposition of ensemble projections. Stacks show the fraction of total variance of midcentury crop production changes (2030–2070 mean) induced by the climate model ensemble (GCMs; yellow) and by the crop model ensemble (GGCMs; pink), for GGCMI–CMIP6 (GC6) and GGCMI–CMIP5 (GC5) under RCP8.5, respectively. Variance fractions are normalized by the variance cross-term to be additive. The absolute variance introduced by GGCMs and GCMs is indicated at the base of each stack. The GCM ensemble has five members in both cases, the GGCM ensemble has 12 members in GC6 and seven members in GC5, which further highlights that the crop model response became more consistent in GC6 compared to the climate model uncertainty.

which are critical for crop modelling. Higher [CO_2] in CMIP6 are due to a revised trade-off between [CO_2] and [CH_4] resulting from updated observations and assumptions in the MAGICC7.0 model[42].

The GGCMI crop model ensemble has substantially changed and consists of revised and new members. For example, LPJmL contributed to GC5 and has since been fundamentally improved with the addition of the nitrogen cycle[43] and heat unit parameterization[44]. In addition, input data and model harmonization have been improved, including growing season harmonization based on a new crop calendar developed for this study (Methods). A comprehensive attribution of crop response differences between GC5 and GC6 to changes in climate forcing, crop model selection and sensitivities, and input data is not feasible. But standardized comparisons of changes in cropland warming and [CO_2] indicate that, for maize and wheat, changes in crop model ensemble sensitivities dominate the response, and for soybean and rice, higher warming levels and warming sensitivity explain much of the differences (Fig. 7 and Supplementary Fig. 7).

The new GCM bias adjustment, crop model advancement, improved input data and a new crop yield bias correction serve to substantially reduce the amount of variance induced by the crop models compared to the climate models, rendering the new GC6 ensemble more balanced and consistent than GC5 despite a larger ensemble size (12 crop models in GC6, 7 in GC5; Fig. 8). In a similar vein, Müller et al.[45] comprehensively compared crop yield uncertainties under all CMIP5 and CMIP6 GCMs based on GGCMI crop model emulators[46], confirming that CMIP6 introduces a wider range of yield responses with more pessimistic average impacts. In view of improved model harmonization, inputs and GGCM versions and performance, we consider GC6 more reliable than GC5—despite ongoing discussions on the temperature sensitivity in CMIP6.

The uncertainty in the mechanisms and overall size of the effects of CO_2 fertilization manifested in farmers' fields are reflected in a wide range of CO_2 sensitivities among the crop models contributing to the GGCMI archive[20]. Average simulated CO_2 fertilization effects are generally in line with field experiments[20,47,48], but the wide range of this effect merits more rigorous model testing at the process level, which in turn requires better reference data, especially at high [CO_2] levels. Moreover, elevated [CO_2] boosts crop yield, but may

also affect the nutritional content of the crops[49,50]. Impacts related to excess moisture, water resource limitations and new distributions of pests and diseases may lead to additional regional biotic stresses requiring follow-on analysis.

Cropping system adaptation can substantially reduce and even outweigh adverse climate change impacts, for example, by switching to other crops[51] or better-adapted varieties[52]. Integrated into ISIMIP's wider cross-sector activities, GGCMI will systematically evaluate farming system adaptation and changes in yield variability and extreme event impacts in subsequent efforts.

In conclusion, the new generation of AgMIP's GGCMI provides the most comprehensive ensemble of process-based future crop yield projections under climate change to date. The degree to which even high mitigation climate change scenarios are projected to push global farming outside of its historical regimes suggests that current food production systems will soon face fundamentally changed risk profiles. Despite prevailing uncertainties, these ensemble projections spotlight the need for targeted food system adaptation and risk management across the main producer regions in the coming decades.

Methods

Time of emergence metric. We define TCIE as the year in which the smoothed climate change signal ('signal') exceeds the underlying internal variability and model uncertainty ('noise'). The signal is the multi-model ensemble mean crop productivity change against the 1983–2013 reference period (smoothed with a 25 yr moving window). Noise is defined as the standard deviation of simulated historical variability of crop productivity across all individual GCM×GGCM combinations (1983–2013). TCIE is the first year in which the signal emerges from the noise, that is, when the signal-to-noise ratio becomes greater than 1. Similar time of emergence definitions have been used in previous studies (for example, refs. [12,14,53,54]). Historical productivity time series are not detrended as we hold all management factors constant throughout the simulations. To assess TCIE uncertainties, we calculate TCIE also for each individual climate–crop model realization as suggested by Hawkins and Sutton[12], and we analyse the distribution of the individual estimates (including mean, median, IQR and s.d.). We find that the multi-model ensemble mean TCIE usually occurs between the median and the mean of individual TCIE estimates. For example, global-level maize production under RCP8.5 shows a multi-model ensemble mean TCIE in year 2032, the median of individual estimates occurs in year 2027 and the mean in year 2036. Wheat shows the same pattern and results are qualitatively the same across the different methods. To test the robustness of results in another way, we calculate the

multi-model ensemble mean TCIE iteratively while removing one crop model at a time. The s.d. of this distribution at global level is marginal; 1.5 yr for both maize and wheat under RCP8.5. As a final metric, we also compare the number of climate and crop model combinations that show an emergence signal by the end of the century. We calculate TCIE at global level, for different Koeppen–Geiger climate zones, and for individual grid cells. Earlier TCIE is generally found for larger spatial scales as the variance of internal variability decreases with averaging. For additional discussions see, for example, refs. [11–13].

ISIMIP climate input datasets. GGCMI simulation efforts for CMIP6 impact assessment are aligned with the ISIMIP[5] activity in which GGCMI represents the agriculture sector. Key modelling inputs such as information on climate, land use, fertilizer input, soils, among others, are harmonized across various research sectors. CMIP6 climate model outputs are centrally bias-adjusted and downscaled by the ISIMIP framework to provide climate-input datasets on a daily regular 0.5° × 0.5° global grid. The bias-adjustment method employs a quantile mapping approach and uses the observational W5E5 v.1.0 dataset[55,56]. This historical dataset compares favourably with climatic forcing datasets that have been used previously by AgMIP GGCMI[57]. The new quantile-mapping method adjusts biases and preserves trends in all quantiles of the distribution of simulated daily climate model outputs; for more details see Lange[10]. To lower the barrier for participation in this study we provide climate input data for five CMIP6 GCMs: GFDL-ESM4, IPSL-CM6A-LR, MPI-ESM1-2-HR, MRI-ESM2-0 and UKESM1-0-LL (see Supplementary Table 1 for further details). The GCM selection is based on data availability at the time of selection, performance in the historical period, structural independence, process representation and equilibrium climate sensitivity (ECS). The five GCMs are structurally independent in terms of their ocean and atmosphere model components and overall they represent the range of ECS across the full CMIP6 ensemble, including three models with below-average ECS (GFDL-ESM4, MPI-ESM1-2-HR and MRI-ESM2-0) and two models with above-average ECS (IPSL-CM6A-LR and UKESM1-0-LL)[8]. ECS and transient climate response (TCR) for all GCMs used are listed in Supplementary Table 1. The mean and s.d. of both ECS (mean, 3.7 °C; s.d., 1.1) and TCR (mean, 2.0 °C; s.d., 0.5) across the five GCMs used here precisely match the mean and s.d. across the full CMIP6 ensemble with 38 members (Supplementary Tables 1 and 2), much better than in GC5, although the range of ECS in the CMIP6 ISIMIP models is larger than in the CMIP5 ISIMIP models.

The daily weather variables at a 0.5° spatial resolution that are used as input for the crop models include: daily mean, minimum, and maximum 2 m air temperature (T, T_{min} and T_{max}, respectively (°C)), daily total precipitation (P (mm)), and daily mean shortwave and longwave radiation (SR and LR (W m^{-2})).

GGCMI phase 3 crop modelling protocol. Bias-adjusted climate model projections are used to drive transient crop model simulations, that is, uninterrupted runs for the historical (1850–2014) and future (2015-2100) time periods. Potential future trajectories are represented by SSP1 with RCP2.6 (here SSP126) and SSP5 with RCP8.5 (here SSP585). Therefore, each crop model performs 20 future simulation runs for each crop (5 GCM × 2 RCP × 2 [CO$_2$] settings). Note that in this study any socioeconomic forcing or adaptation effort associated with the SSP storylines is held constant at the year 2015 level to isolate the climate signal (that is, year 2015 land-use, fertilizer application, growing seasons, crop cultivars, but also NO$_3$ and NH$_4$ deposition rates, are used in years after 2015). To help isolate yield effects associated with the CO$_2$ fertilization effect, all crop model simulations are run for two separate assumptions: (1) transient [CO$_2$] in line with the respective RCP ('default [CO$_2$]'), and (2) [CO$_2$] concentration held constant at the 2015 level at 399.95 ppmv ('constant [CO$_2$]'). Differences between the two [CO$_2$] levels are not a measure of [CO$_2$] uncertainty, as there is no plausible climate change scenario without increasing [CO$_2$][22]. Instead, this set-up is used to quantify the size of the CO$_2$ fertilization effect and for climate change factor attribution. All simulations are carried out at the 0.5° global grid. In addition to the GCM forcing, we include historical simulations based on the reanalysis product GSWP3-W5E5 v.1.0[55,56] for each crop model and crop to better evaluate crop model performance against observational data.

We focus on the four major global grain crops, that is, maize (*Zea mays* L.), wheat (*Triticum* sp. L.), rice (*Oryza sativa* L.) and soybean (*Glycine max* L. Merr.). Wheat is simulated as winter and spring wheat individually; grain and silage maize are not distinguished. These four main crops contribute 90% of today's global caloric production of all cereals and soybean[58].

All crops are simulated under both rainfed conditions and full irrigation (where soil moisture is set to field capacity every day, without constraints on water availability) in all grid cells—independent of the current cropland distribution. The physical cropland extent is applied in postprocessing based on the MIRCA2000 (Monthly Irrigated and Rainfed Crop Areas around the year 2000) reference dataset[59] and irrigated fractions are adapted from Siebert et al.[60]; both are held constant over time.

Soil moisture and soil temperature for various soil layers are calculated by most crop models in a transient way, that is, without reinitializing at the beginning of each year. All models use a classic phenological heat sum approach to determine physiological stages between planting and maturity. Heat unit accumulation can be modified by the sensitivity to day length (photoperiod) and for winter wheat is stalled until vernalization requirements are reached, that is, the exposure to cold temperatures before anthesis. Planting dates (Crop calendar and crop varieties) are constant over time but the heat sum approach leads to different growing season lengths depending on the daily temperature distribution in each growing season. Except for rice, we simulate only one growing season per calendar year. The first and last years of the transient runs are removed from crop model simulations due to partially incomplete growing seasons. Simulations in grid cells with a growing season length <50 d are removed, as are simulations resulting in premature harvest (that is, accumulated heat units <80% of required heat units; this applies only to those models that can provide such outputs).

The harmonization of crop models includes the required use of a central crop calendar product (new development for this study, see below), fertilizer inputs and soil information. Additional protocol characteristics are recommended but not required, as not all models can address all features (see below).

Simulation protocols determine mineral and organic fertilizer (kgN ha^{-1}) inputs per crop and grid cell. Mineral fertilizer (ammonium nitrate; NH$_4$NO$_3$) application is crop specific and is derived from the LUH2 product[61], harmonized by ISIMIP and GGCMI. Manure application inputs (C:N ratio, 14.5) are grid cell specific, but constant across crops[62]. All other nutrients are considered non-limiting. Fertilizer scheduling follows a simple assumption with 20% applied at sowing and 80% applied when 25% of the heat units required to reach maturity are accumulated. As for all other management aspects, fertilizer application is held constant throughout the simulation period. Atmospheric nitrogen deposition is considered, separating NH$_x$ and NO$_y$, based on Tian et al.[63] and held constant at the 2015 level.

Soil input is harmonized across crop models for the first time in GGCMI, derived from the Harmonized World Soil Database (HWSD)[64]. While the same HWSD dataset is used across ISIMIP sectors, in this study we employ a different algorithm to aggregate the data to 0.5° in order to be cropland specific. The pDSSAT model uses the Global Soil Data set for Earth system modelling (GSDE)[65] and DSSAT-Pythia uses the Global High-Resolution Soil Profile Database for Crop Modelling Applications[66] due to difficulties in retrieving all soil parameters from HWSD.

Finally, the following management aspects are encouraged to be harmonized across crop models, but are not accounted for by all teams: tillage (two tillage events, planting day and harvest day, 200 mm depth, full inversion), residues (70% of above-ground residues removed), no pest and disease damage, no soil erosion and no cover crops. Except for rice and wheat, which are simulated for two separate growing seasons, we do not consider multicropping systems or crop rotations. Inputs are provided for 18 different crops globally, but most crop models can only simulate the major crops, which we focus on in this study. All socioeconomic and farm management input data are publicly available via www.isimip.org.

Participating GGCMI crop models. Twelve process-based global crop models participate in this study: ACEA, CROVER, CYGMA1p74, DSSAT-Pythia, EPIC-IIASA, ISAM, LandscapeDNDC, LPJmL, pDSSAT, PEPIC, PROMET and SIMPLACE-LINTUL5 (see Supplementary Table 3 for further details and references). The full ensemble, therefore, consists of roughly 240 future crop model simulations per crop plus one historical reference run for each crop and climate model and one historical reanalysis run per crop model. Due to computational constraints, ACEA has only run GCMs UKESM1-0-LL and MRI-ESM2-0 so far, and DSSAT-Pythia has not yet run UKESM1-0-LL. ACEA and DSSAT-Pythia have not yet finished simulations for the constant [CO$_2$] setting.

All crop models are considered independent. LPJmL, pDSSAT, EPIC-IIASA, PROMET and PEPIC have participated in previous GGCMI protocols[7,67–69], but the individual models and their parameterizations have substantially advanced. This is especially the case for those models that participated in GC5 and GC6 (LPJmL, pDSSAT, EPIC-based models) and a comprehensive account of changes in the model code, parameters, inputs and the modelling protocol is beyond the scope of this study. The main structural differences for LPJmL include the addition of a nitrogen cycle, crop residue and tillage management, and manure application; PEPIC and EPIC-IIASA in GC6 used the Penman–Monteith method to estimate PET, GEPIC and EPIC in GC5 used the Hargreaves method and more generally a substantially different model parameterization and spin-up protocol. In GC5 pDSSAT used DSSAT4.0 and different yield and cultivar calibrations. As opposed to GC6, in GC5 fertilizer application rates and timing, planting and harvest dates, soil information, irrigation and soil erosion were not harmonized across modelling teams.

While the other models are new GGCMI ensemble members, they have been thoroughly evaluated individually (see references in Supplementary Table 3). To participate in this study, each model was required to go through a benchmark performance evaluation for the historical period based on GSWP3-W5E5 reanalysis data (results available upon request). An overview of the degree to which the GC6 crop models explain observed interannual yield variability is presented in Supplementary Fig. 10. For the top five producer countries per crop, the ensemble mean generally shows higher performance in terms of correlation and root-mean-square error than the bulk of individual models. Generally, explained

variability in individual models is satisfactory for most maize, wheat and soybean main-producer countries. The metrics are lower for rice which also links to the fact that the weather signal in (largely irrigated) rice is smaller than in other crops, and the overall observed interannual variability in these rice producer countries is smaller than for the other crops. Since management decisions (planting dates, crop rotations and areas, fertilizer application, irrigation and so on) are held constant over time, the crop models can only capture the interannual weather signal in reported yields, which in general is much smaller in the tropics compared to mid- to high-latitude regions. Additional in-depth GGCMI model comparison and evaluation is presented by Müller et al.[67]. Overall, crop model performance evaluation based on historical yield variability provides limited insight into the models' capability to project future yield impacts[70].

Since GCM-based crop model simulations are difficult to compare with observed interannual yield levels (for example, the 1988 drought does not necessarily occur in 1988 in the GCM), we compare the overall range of simulated and observed yield variability across the historical reference period. The standard deviation of observed national yield variability is matched to a substantially higher degree in GC6 ($R = 79\%$, r.m.s.e. $= 0.11$) than in GC5 ($R = 44\%$, r.m.s.e. $= 0.17$), which is indicative of more realistic yield responses in GC6 (Supplementary Fig. 9). These improvements are linked to a combination of factors, including different internal variability in CMIP6, new GCM bias-adjustment method, improved crop model ensemble, new crop yield bias-correction and improved crop model inputs. The match with observed yield variability using GC6 simulations based on GSWP3-W5E5 reanalysis data is only slightly better ($R = 87\%$, r.m.s.e. $= 0.09$) than with GCM-forced simulations, which highlights that the CMIP6 GCMs do not introduce substantial errors in terms of historical variability (Supplementary Fig. 9).

While the models generally reproduce yield declines in extreme years, adverse impacts of excess water on crop growth due to lower aeration, waterlogging and nitrogen leaching are generally underrepresented in current global crop models[32]. As an exception, the crop model CYGMA accounts for effects due to excess moisture stress[71]. ACEA, EPIC-based, and DSSAT-based crop models also have processes related to waterlogging and root aeration but associated stresses occur rarely and foremost on sensitive soils[72]. Many models do not handle direct effects of extreme heat (for example, on leaf senescence, pollen sterility; see Supplementary Table 3)[3]. Individual model responses to elevated [CO_2] are shown in Fig. 7 and Supplementary Fig. 8 and discussed in the main text. The ISAM model requires sub-daily weather data and therefore uses CRU–National Centers for Environmental Prediction (CRUNCEP) diurnal factors to convert daily bias-adjusted climate model data to diurnal data. The PROMET model also requires sub-daily weather data and uses ERA5-derived diurnal factors to convert climate model data to diurnal inputs; it also uses WFDE5 instead of GSWP3-W5E5 for reanalysis simulations.

All models use spin-up simulations of various lengths to reach soil and carbon pool equilibrium. EPIC-IIASA uses dynamic soil handling during spin-up to generate soil attributes. Subsequently these are used as an input in the actual simulations with static soil handling, that is annual reinitialization of all soil attributes (including soil organic matter fractions and soil texture among others) except mineral nutrient pools, temperature and soil moisture. The models do not account for human management intervention other than fertilizer application, irrigation, seed selection, growing periods and basic field management such as tillage and residue removal.

All models follow a phenology calibration with respect to grid cell-specific cultivar parameterizations (that is, phenological heat units) based on the respective crop calendar and weather forcing (Supplementary Table 3). Yield calibration is not harmonized across crop models and each team follows their individual protocol, including grid cell-specific calibration against SPAM[73] reference yields (for example, pDSSAT), various site-specific efforts based on field experiments (for example, ISAM) and calibrations with national FAO[58] statistics (for example, PEPIC).

Crop yield bias correction. Crop production is calculated as yield times harvested area of the respective crop. We omit grid cells with <10 ha cropland area for each crop. To compare results across crop models, but also to represent realistic overall crop production estimates and spatial pattern, we calculate fractional yield changes from each individual crop model simulation between the historical reference period (1983–2013) and the respective future projection and multiply these with a spatially explicit (0.5°) observational yield reference dataset (see Supplementary Fig. 14 in ref. [74]). SPAM (Spatial Production Allocation Model)[73] is used as the main reference yield data as it separates rainfed and irrigated systems. Grid cells with missing SPAM yield data but with >10 ha MIRCA2000 harvested area are gap-filled with Ray et al.[75] yield data; both SPAM and Ray et al. represent the time period 2003 to 2007.

Crop calendar and crop varieties. We provide planting and maturity dates for each crop in each grid cell, separate for rainfed and irrigated systems, based on a new observational crop calendar product. See Supplementary Information section GGCMI crop calendar and Supplementary Figs. 11-14 for details. Growing season inputs are static over time throughout the historical and future time period to avoid confounding trends. Each model calculated required reference heat units to reach physiological maturity for each crop in each grid cell by averaging annual heat sums over all growing seasons between 1979 and 2010.

Map projection and smoothing. Global maps are based on the Robinson projection and grid-level data are smoothed to improve clarity and visual appearance. Smoothing is done by first resampling the raw data to five times finer resolution, followed by a 5 × 5 grid cell focal mean window aggregation. Map smoothing is done for visualization purposes only and all analyses are based on the raw data.

Reporting summary. Further information on research design is available in the Nature Research Reporting Summary linked to this article.

Data availability

All data needed to evaluate the conclusions in the paper are present in the paper and/or the Supplementary Information. Model inputs are publicly available via https://www.isimip.org/ or from the corresponding author. The GGCMI crop calendar is accessible at https://doi.org/10.5281/zenodo.5062513; fertilizer inputs are available at https://doi.org/10.5281/zenodo.4954582. Crop model simulations will be made publicly available under the CC0 license pending publication.

Code availability

Details and code for each crop model can be requested from the contact persons listed in Supplementary Table 3. Code developed for data analysis and figures is available from the corresponding author upon request.

References

1. Mbow, C. et al. in *Special Report on Climate Change and Land* (eds Shukla, P. R. et al.) 437–550 (IPCC, 2019).
2. Asseng, S. et al. Uncertainty in simulating wheat yields under climate change. *Nat. Clim. Change* **3**, 827–832 (2013).
3. Wang, E. et al. The uncertainty of crop yield projections is reduced by improved temperature response functions. *Nat. Plants* **3**, 17102 (2017).
4. Rosenzweig, C. et al. The agricultural model intercomparison and improvement project (AgMIP): protocols and pilot studies. *Agric. For. Meteorol.* **170**, 166–182 (2013).
5. *The Inter-Sectoral Impact Model Intercomparison Project* (ISIMIP, 2021); https://www.isimip.org/
6. Eyring, V. et al. Overview of the Coupled Model Intercomparison Project phase 6 (CMIP6) experimental design and organization. *Geosci. Model Dev.* **9**, 1937–1958 (2016).
7. Rosenzweig, C. et al. Assessing agricultural risks of climate change in the 21st century in a Global Gridded Crop Model intercomparison. *Proc. Natl Acad. Sci. USA* **111**, 3268–3273 (2014).
8. Meehl, G. A. et al. Context for interpreting equilibrium climate sensitivity and transient climate response from the CMIP6 Earth system models. *Sci. Adv.* **6**, eaba1981 (2020).
9. O'Neill, B. C. et al. The Scenario Model Intercomparison Project (ScenarioMIP) for CMIP6. *Geosci. Model Dev.* **9**, 3461–3482 (2016).
10. Lange, S. Trend-preserving bias adjustment and statistical downscaling with ISIMIP3BASD (v1.0). *Geosci. Model Dev.* **12**, 3055–3070 (2019).
11. Hawkins, E. et al. Observed emergence of the climate change signal: from the familiar to the unknown. *Geophys. Res. Lett.* **47**, e2019GL086259 (2020).
12. Hawkins, E. & Sutton, R. Time of emergence of climate signals. *Geophys. Res. Lett.* **39**, L01702 (2012).
13. Kirtman, B. et al. in *Climate Change 2013: The Physical Science Basis* (eds Stocker, T. F. et al.) 953–1028 (IPCC, Cambridge Univ. Press, 2013).
14. Rojas, M., Lambert, F., Ramirez-Villegas, J. & Challinor, A. J. Emergence of robust precipitation changes across crop production areas in the 21st century. *Proc. Natl Acad. Sci. USA* **116**, 6673–6678 (2019).
15. Raymond, C., Matthews, T. & Horton, R. M. The emergence of heat and humidity too severe for human tolerance. *Sci. Adv.* **6**, eaaw1838 (2020).
16. Park, C. E. et al. Keeping global warming within 1.5 °C constrains emergence of aridification. *Nat. Clim. Change* https://doi.org/10.1038/s41558-017-0034-4 (2018).
17. Liu, B. et al. Similar estimates of temperature impacts on global wheat yield by three independent methods. *Nat. Clim. Change* **6**, 1130–1136 (2016).
18. Zhao, C. et al. Temperature increase reduces global yields of major crops in four independent estimates. *Proc. Natl Acad. Sci. USA* https://doi.org/10.1073/pnas.1701762114 (2017).
19. Asseng, S. et al. Rising temperatures reduce global wheat production. *Nat. Clim. Change* **5**, 143–147 (2014).
20. Toreti, A. et al. Narrowing uncertainties in the effects of elevated CO_2 on crops. *Nat. Food* **1**, 775–782 (2020).

21. Ahmed, M. et al. Novel multimodel ensemble approach to evaluate the sole effect of elevated CO_2 on winter wheat productivity. *Sci. Rep.* **9**, 7813 (2019).

22. Leakey, A. D. B., Bishop, K. A. & Ainsworth, E. A. A multi-biome gap in understanding of crop and ecosystem responses to elevated CO_2. *Curr. Opin. Plant Biol.* https://doi.org/10.1016/j.pbi.2012.01.009 (2012).

23. Kimball, B. A. Crop responses to elevated CO_2 and interactions with H_2O, N, and temperature. *Curr. Opin. Plant Biol.* https://doi.org/10.1016/j.pbi.2016.03.006 (2016).

24. Zabel, F. et al. Large potential for crop production adaptation depends on available future varieties. *Glob. Change Biol.* https://doi.org/10.1111/gcb.15649 (2021).

25. Ray, D. K. et al. Climate change has likely already affected global food production. *PLoS ONE* **14**, e0217148 (2019).

26. Lobell, D. B., Schlenker, W. & Costa-Roberts, J. Climate trends and global crop production since 1980. *Science* **333**, 616–620 (2011).

27. Ahmad, S. et al. Climate warming and management impact on the change of phenology of the rice–wheat cropping system in Punjab, Pakistan. *Field Crops Res.* **230**, 46–61 (2019).

28. Porter, J. R. et al. in *Climate Change 2014: Impacts, Adaptation, and Vulnerability* (eds Field, C. B. et al.) 485–533 (IPCC, Cambridge Univ. Press, 2014).

29. Levis, S., Badger, A., Drewniak, B., Nevison, C. & Ren, X. CLMcrop yields and water requirements: avoided impacts by choosing RCP 4.5 over 8.5. *Clim. Change* **146**, 501–515 (2018).

30. Falconnier, G. N. et al. Modelling climate change impacts on maize yields under low nitrogen input conditions in sub-Saharan Africa. *Glob. Change Biol.* **26**, 5942–5964 (2020).

31. O'Neill, B. C. et al. IPCC reasons for concern regarding climate change risks. *Nat. Clim. Change* **7**, 28–37 (2017).

32. Li, Y., Guan, K., Schnitkey, G. D., DeLucia, E. & Peng, B. Excessive rainfall leads to maize yield loss of a comparable magnitude to extreme drought in the United States. *Glob. Change Biol.* **25**, 2325–2337 (2019).

33. Zhu, P., Zhuang, Q., Archontoulis, S. V., Bernacchi, C. & Müller, C. Dissecting the nonlinear response of maize yield to high temperature stress with model-data integration. *Glob. Change Biol.* **25**, 2470–2484 (2019).

34. Iizumi, T. et al. Responses of crop yield growth to global temperature and socioeconomic changes. *Sci. Rep.* **7**, 7800 (2017).

35. Sherwood, S. C. et al. An assessment of Earth's climate sensitivity using multiple lines of evidence. *Rev. Geophys.* **58**, e2019RG000678 (2020).

36. Nijsse, F. J. M. M., Cox, P. M. & Williamson, M. S. Emergent constraints on transient climate response (TCR) and equilibrium climate sensitivity (ECS) from historical warming in CMIP5 and CMIP6 models. *Earth Syst. Dyn.* **11**, 737–750 (2020).

37. Zelinka, M. D. et al. Causes of higher climate sensitivity in CMIP6 models. *Geophys. Res. Lett.* **47**, e2019GL085782 (2020).

38. Tokarska, K. B. et al. Past warming trend constrains future warming in CMIP6 models. *Sci. Adv.* **6**, eaaz9549 (2020).

39. Fan, X., Miao, C., Duan, Q., Shen, C. & Wu, Y. The performance of CMIP6 versus CMIP5 in simulating temperature extremes over the global land surface. *J. Geophys. Res. Atmos.* **125**, e2020JD033031 (2020).

40. Xin, X., Wu, T., Zhang, J., Yao, J. & Fang, Y. Comparison of CMIP6 and CMIP5 simulations of precipitation in China and the East Asian summer monsoon. *Int. J. Climatol.* **40**, 6423–6440 (2020).

41. Ridder, N. N., Pitman, A. J. & Ukkola, A. M. Do CMIP6 climate models simulate global or regional compound events skilfully? *Geophys. Res. Lett.* https://doi.org/10.1029/2020gl091152 (2020).

42. Meinshausen, M. et al. The shared socio-economic pathway (SSP) greenhouse gas concentrations and their extensions to 2500. *Geosci. Model Dev.* **13**, 3571–3605 (2020).

43. Von Bloh, W. et al. Implementing the nitrogen cycle into the dynamic global vegetation, hydrology, and crop growth model LPJmL (version 5.0). *Geosci. Model Dev.* **11**, 2789–2812 (2018).

44. Jägermeyr, J. & Frieler, K. Spatial variations in crop growing seasons pivotal to reproduce global fluctuations in maize and wheat yields. *Sci. Adv.* **4**, eaat4517 (2018).

45. Müller, C. et al. Exploring uncertainties in global crop yield projections in a large ensemble of crop models and CMIP5 and CMIP6 climate scenarios. *Environ. Res. Lett.* **16**, 034040 (2021).

46. Franke, J. A. et al. The GGCMI Phase 2 emulators: Global Gridded Crop Model responses to changes in CO2, temperature, water, and nitrogen (version 1.0). *Geosci. Model Dev.* **13**, 2315–2336 (2020).

47. Allen, L. H. et al. Fluctuations of CO_2 in free-air CO_2 enrichment (FACE) depress plant photosynthesis, growth, and yield. *Agric. For. Meteorol.* **284**, 107899 (2020).

48. Durand, J. L. et al. How accurately do maize crop models simulate the interactions of atmospheric CO_2 concentration levels with limited water supply on water use and yield? *Eur. J. Agron.* https://doi.org/10.1016/j.eja.2017.01.002 (2018).

49. Myers, S. S. et al. Increasing CO_2 threatens human nutrition. *Nature* **510**, 139–142 (2014).

50. Zhu, C. et al. Carbon dioxide (CO_2) levels this century will alter the protein, micronutrients, and vitamin content of rice grains with potential health consequences for the poorest rice-dependent countries. *Sci. Adv.* **4**, eaaq1012 (2018).

51. Rising, J. & Devineni, N. Crop switching reduces agricultural losses from climate change in the United States by half under RCP 8.5. *Nat. Commun.* **11**, 4991 (2020).

52. Asseng, S. et al. Climate Change impact and adaptation for wheat protein. *Glob. Change Biol.* **25**, 155–173 (2019).

53. Hawkins, E. & Sutton, R. The potential to narrow uncertainty in regional climate predictions. *Bull. Am. Meteorol. Soc.* **90**, 1095–1107 (2009).

54. Giorgi, F. & Bi, X. Time of emergence (TOE) of GHG-forced precipitation change hot-spots. *Geophys. Res. Lett.* **36**, L06709 (2009).

55. Lange, S. *WFDE5 Over Land Merged with ERA5 Over the Ocean (W5E5)*. V. 1.0 (GFZ Data Services, 2019); https://doi.org/10.5880/pik.2019.023

56. Cucchi, M. et al. WFDE5: bias-adjusted ERA5 reanalysis data for impact studies. *Earth Syst. Sci. Data* **12**, 2097–2120 (2020).

57. Ruane, A. C. et al. Strong regional influence of climatic forcing datasets on global crop model ensembles. *Agric. For. Meteorol.* **300**, 108313 (2021).

58. FAOSTAT (United Nation's Food and Agricultural Organization, 2019); http://www.fao.org/faostat/

59. Portmann, F. T., Siebert, S. & Döll, P. MIRCA2000—Global monthly irrigated and rainfed crop areas around the year 2000: a new high-resolution data set for agricultural and hydrological modeling. *Global Biogeochem. Cycles* **24**, GB1011 (2010).

60. Siebert, S. et al. A global data set of the extent of irrigated land from 1900 to 2005. *Hydrol. Earth Syst. Sci.* **19**, 1521–1545 (2015).

61. Heinke, J., Müller, C., Mueller, N. D. & Jägermeyr, J. N application rates from mineral fertiliser and manure *Zenodo* https://doi.org/10.5281/zenodo.4954582 (2021).

62. Zhang, B. et al. Global manure nitrogen production and application in cropland during 1860–2014: a 5 arcmin gridded global dataset for Earth system modeling. *Earth Syst. Sci. Data* **9**, 667–678 (2017).

63. Tian, H. et al. The global N_2O model intercomparison project. *Bull. Am. Meteorol. Soc.* **99**, 1231–1251 (2018).

64. Nachtergaele, F. et al. *Harmonized World Soil Database (version 1.2)* (FAO and IIASA, 2012).

65. Shangguan, W., Dai, Y., Duan, Q., Liu, B. & Yuan, H. A global soil data set for Earth system modeling. *J. Adv. Model. Earth Syst.* **6**, 249–263 (2014).

66. Hengl, T. et al. SoilGrids1km—global soil information based on automated mapping. *PLoS ONE* **9**, e114788 (2014).

67. Müller, C. et al. Global Gridded Crop Model evaluation: benchmarking, skills, deficiencies and implications. *Geosci. Model Dev.* **10**, 1403–1422 (2017).

68. Franke, J. A. et al. The GGCMI Phase 2 experiment: Global Gridded Crop Model simulations under uniform changes in CO_2, temperature, water, and nitrogen levels (protocol version 1.0). *Geosci. Model Dev.* **13**, 2315–2336 (2020).

69. Elliott, J. et al. The Global Gridded Crop Model Intercomparison: data and modeling protocols for Phase 1 (v1.0). *Geosci. Model Dev.* **8**, 261–277 (2015).

70. Ruane, A. C. et al. Multi-wheat-model ensemble responses to interannual climate variability. *Environ. Model. Softw.* **81**, 86–101 (2016).

71. Wang, R., Bowling, L. C. & Cherkauer, K. A. Estimation of the effects of climate variability on crop yield in the Midwest USA. *Agric. For. Meteorol.* **216**, 141–156 (2016).

72. Folberth, C., Gaiser, T., Abbaspour, K. C., Schulin, R. & Yang, H. Regionalization of a large-scale crop growth model for sub-Saharan Africa: model setup, evaluation, and estimation of maize yields. *Agric. Ecosyst. Environ.* **151**, 21–33 (2012).

73. *Global Spatially-Disaggregated Crop Production Statistics Data for 2010 Version 1.0.* Harvard Dataverse, V1 (International Food Policy Research Institute, 2019); https://doi.org/10.7910/DVN/PRFF8V

74. Jägermeyr, J. et al. A regional nuclear conflict would compromise global food security. *Proc. Natl Acad. Sci. USA* **117**, 7071–7081 (2020).

75. Ray, D. K., Ramankutty, N., Mueller, N. D., West, P. C. & Foley, J. A. Recent patterns of crop yield growth and stagnation. *Nat. Commun.* **3**, 1293 (2012).

Acknowledgements

Author contributions

J.J. and C.M. conceived the paper and coordinated GGCMI. J.J., C.M. and S.S.R. developed the simulation protocol. A.C.R. and C.R. coordinated AgMIP integration. C.M., J.J., J.B., O.C., B.F., C.F., K.F., G.H., T.I., A.K.J., N.K., T.-S.L., W.L., S.M., M.O., O.M., C.P., S.S.R., J.M.S., J.F.S., R.S., A.S., T.S. and F.Z. conducted crop model simulations. S.L. prepared climate data inputs. J.J. conducted the data analysis, and developed the manuscript and figures. All coauthors supported manuscript writing.

Competing interests

The authors declare no competing interests.

Additional information

Supplementary information The online version contains supplementary material available at https://doi.org/10.1038/s43016-021-00400-y.

Correspondence and requests for materials should be addressed to Jonas Jägermeyr.

Peer review information *Nature Food* thanks Bin Peng and the other, anonymous, reviewer(s) for their contribution to the peer review of this work.

Reprints and permissions information is available at www.nature.com/reprints.

Publisher's note Springer Nature remains neutral with regard to jurisdictional claims in published maps and institutional affiliations.

nature research

Corresponding author(s): Jonas Jägermeyr

Last updated by author(s): 9/3014/21

Reporting Summary

Nature Research wishes to improve the reproducibility of the work that we publish. This form provides structure for consistency and transparency in reporting. For further information on Nature Research policies, see our Editorial Policies and the Editorial Policy Checklist.

Statistics

For all statistical analyses, confirm that the following items are present in the figure legend, table legend, main text, or Methods section.

n/a	Confirmed	
☐	☒	The exact sample size (*n*) for each experimental group/condition, given as a discrete number and unit of measurement
☒	☐	A statement on whether measurements were taken from distinct samples or whether the same sample was measured repeatedly
☐	☒	The statistical test(s) used AND whether they are one- or two-sided *Only common tests should be described solely by name; describe more complex techniques in the Methods section.*
☒	☐	A description of all covariates tested
☒	☐	A description of any assumptions or corrections, such as tests of normality and adjustment for multiple comparisons
☐	☒	A full description of the statistical parameters including central tendency (e.g. means) or other basic estimates (e.g. regression coefficient) AND variation (e.g. standard deviation) or associated estimates of uncertainty (e.g. confidence intervals)
☒	☐	For null hypothesis testing, the test statistic (e.g. *F*, *t*, *r*) with confidence intervals, effect sizes, degrees of freedom and *P* value noted *Give P values as exact values whenever suitable.*
☒	☐	For Bayesian analysis, information on the choice of priors and Markov chain Monte Carlo settings
☒	☐	For hierarchical and complex designs, identification of the appropriate level for tests and full reporting of outcomes
☒	☐	Estimates of effect sizes (e.g. Cohen's *d*, Pearson's *r*), indicating how they were calculated

Our web collection on statistics for biologists contains articles on many of the points above.

Software and code

Policy information about availability of computer code

Data collection	Crop models contributing data to the study are written in various languages including C, Python, Fortran, etc. Details and code for each model can be requested from the respective contact person listed in the Supplement.
Data analysis	All data analyses and the preparation of figures are done using R version 3.6.2 (Copyright (C) 2019 The R Foundation for Statistical Computing, Platform: x86_64-pc-linux-gnu (64-bit)).

For manuscripts utilizing custom algorithms or software that are central to the research but not yet described in published literature, software must be made available to editors and reviewers. We strongly encourage code deposition in a community repository (e.g. GitHub). See the Nature Research guidelines for submitting code & software for further information.

Data

Policy information about availability of data

All manuscripts must include a data availability statement. This statement should provide the following information, where applicable:
- Accession codes, unique identifiers, or web links for publicly available datasets
- A list of figures that have associated raw data
- A description of any restrictions on data availability

All data needed to evaluate the conclusions in the paper are present in the paper and/or the Supplementary Materials. Model inputs are publicly available via https://www.isimip.org/ or from the corresponding author. The GGCMI crop calendar is accessible under the DOI: 10.5281/zenodo.5062513, fertilizer inputs under the DOI: 10.5281/zenodo.4954582. Crop model simulations will be made publicly available under the CC0 license pending publication."

Field-specific reporting

Please select the one below that is the best fit for your research. If you are not sure, read the appropriate sections before making your selection.

☐ Life sciences ☐ Behavioural & social sciences ☒ Ecological, evolutionary & environmental sciences

For a reference copy of the document with all sections, see nature.com/documents/nr-reporting-summary-flat.pdf

Ecological, evolutionary & environmental sciences study design

All studies must disclose on these points even when the disclosure is negative.

Study description	Five climate models provide inputs for an ensemble of harmonized global crop models to simulate potential responses of crop productivity to climate change.
Research sample	Five global climate models from the Coupled Model Intercomparison Project (CMIP) phase 6 are bias-adjusted and downscaled by ISIMIP. The ensemble of GGCMI global process-based crop models samples a range of state-of-the-art dynamic modeling approaches.
Sampling strategy	Climate models were selected by ISIMIP based on benchmark performance, equilibrium climate sensitivity, and output availability. Crop model participation is based on an open call to the GGCMI community, all submissions are considered.
Data collection	Crop model simulations provide the data for the study.
Timing and spatial scale	Crop model simulations run from the year 1850 until 2100 with global coverage and 0.5° spatial resolution.
Data exclusions	No data were excluded.
Reproducibility	Modeling experiments are numerically reproducible, given the archived model version and input data set.
Randomization	Not relevant, data are not grouped and all data are shown.
Blinding	Not relevant, process-based models are equally-weighted independent approaches.

Did the study involve field work? ☐ Yes ☒ No

Reporting for specific materials, systems and methods

We require information from authors about some types of materials, experimental systems and methods used in many studies. Here, indicate whether each material, system or method listed is relevant to your study. If you are not sure if a list item applies to your research, read the appropriate section before selecting a response.

Materials & experimental systems

n/a	Involved in the study
☒ ☐	Antibodies
☒ ☐	Eukaryotic cell lines
☒ ☐	Palaeontology and archaeology
☒ ☐	Animals and other organisms
☒ ☐	Human research participants
☒ ☐	Clinical data
☒ ☐	Dual use research of concern

Methods

n/a	Involved in the study
☒ ☐	ChIP-seq
☒ ☐	Flow cytometry
☒ ☐	MRI-based neuroimaging